Commercial, High-Impact Polypropylenes: Composition and Chain Structure as Revealed by Temperature-Gradient Extraction Fractionation

Hossein Mahdavi, Mojtaba Enayati Nook

School of Chemistry, University College of Science, University of Tehran, P. O. Box 14155-6455, Tehran, Iran

Received 4 April 2011; accepted 7 September 2011
DOI 10.1002/app.35637
Published online 16 January 2012 in Wiley Online Library (wileyonlinelibrary.com).

ABSTRACT: Four different grades of commercial, high-impact polypropylene (hiPP) were fractionated by temperature-gradient extraction fractionation, and the chain structure and melting behavior of the fractions were studied by Fourier transform infrared spectroscopy and differential scanning calorimetry. Furthermore, the morphology of the disperse phase in the resins was characterized by scanning electron microscopy of the microtome-cut etched and original samples. The results show that there was a strong relation between the chain structure, content, and distribution of the dispersed phase and the mechanical properties of hiPP. These parameters of the elastomeric phase are really critical in reaching the best rigidity-impact balance in hiPP. © 2012 Wiley Periodicals, Inc. J Appl Polym Sci 125: 1606–1615, 2012

Key words: fractionation of polymers; morphology; polyolefins

INTRODUCTION

Isotactic polypropylene (iPP) is one of the most important commodity polymers; it has many applications because of its good mechanical properties and favorable cost-to-performance ratio. Despite its good mechanical properties, the brittleness and low impact properties of polypropylene (PP) in low temperatures seriously limit its applications.[1] This drawback of iPP has been well known for a long time, and a variety of techniques are available to eliminate it; these mainly focus on improving iPP's toughness.[2–6] Some of these methods include the blending of iPP with rubbers,[7] the addition of nucleating agents to reduce the average size of iPP spherulites,[8,9] and copolymerization with ethylene.[10] The latter approach, however, is the best method for toughening iPP with respect to both the polymer properties and production cost.[11,12]

There are some industrial processes for the copolymerization of propylene with ethylene in a two-reactor system, such as the Catalloy and Spheripol techniques of Montell and Himont.[13,14] In these processes, the homopolymerization of propylene proceeds in the first reactor with a spherical superactive $TiCl_4/MgCl_2$-based catalyst; then, polymer particles are transferred into the second reactor, where ethylene is introduced to be copolymerized with propylene.

Because active site types on the catalyst differ in their propagation/transfer ratios and comonomer reactivity ratios, in the second reactor, a variety of ethylene–propylene copolymers, from completely amorphous ethylene–propylene random copolymers (EPRs) to semicrystalline ethylene–propylene block copolymers, are formed and finely dispersed in the cavities of the preformed iPP particles.

The high-impact polypropylene (hiPP) produced in this two-reactor system (called *in situ* or *in reactor blend/alloy*) is a mixture of multiple components with a complex structure and a high-tech commodity polymer with a yearly increase of 10%.[15]

The microstructures of polyolefin alloys mainly determine their properties and applications. Therefore, the determination of the complete molecular structure and morphological analysis of such polymers is a desirable task, and a variety of techniques has been applied to accomplish this work.

There have been many structural studies of hiPP that have investigated the composition of blends with different fractionation methods, such as temperature-rising elution fractionation (TREF)[16,17] and temperature-gradient extraction fractionation (TGEF).[18,19] Structural studies also have analyzed the chain structure of the resin (mostly of its fractions) with infrared spectroscopy,[20,21] NMR spectroscopy,[22,23] thermal analysis, and other common methods.[24,25]

Morphological studies of hiPP have mainly aimed to clarify two aspects: (1) the architecture of the iPP

Correspondence to: H. Mahdavi (hmahdavi@khayam.ut.ac.ir).

TABLE I
Some Physical and Mechanical Properties of the iPP and hiPP Samples

Characteristic	iPP (PI0800)	hiPP (EPC40R)	hiPP (EPD60R)	hiPP (1752HL23)	hiPP (108MF10)	Comments
Density	0.910 g/cm^3	0.900 g/cm^3	0.900 g/cm^3	0.900 g/cm^3	0.905 g/cm^3	ASTM D 1505 (ISO 1183)
Melt flow rate	8 g/10 min	7 g/10 min	0.35 g/10 min	15 g/10 min	10 g/10 min	230°C, 2.16 kg, ASTM D 1238 (ISO 1133)
Tensile strength at yield	32 MPa	27 MPa	27 MPa	23 MPa	19 MPa	ASTM D 638
Tensile elongation at yield	11%	12%	15%	—	—	ASTM D 638
Flexural modulus (procedure B)	1.55 GPa	1.35 GPa	1.10 GPa	1.10 GPa	0.95 GPa	ASTM D 790 (ISO 178)
Izod impact, notched	20 J/m	95 J/m	600 J/m	90 J/m[a]	No break	At 23°C, ASTM D 256
Izod impact, notched	—	—	—	60 J/m[a]	No break	At 0°C; ASTM D 256
Izod impact, notched	—	40 J/m	70 J/m	—	100 J/m	At −20°C, ASTM D 256
Rockwell hardness (R scale)	103	84	76	—	62[b]	ASTM D 785 (ISO 868)
Heat Deflection Temperature (HDT) (0.46 N/mm^2)	—	88°C	82°C	90°C	80°C	ASTM D 648 (ISO 75-2/B)
Vicat softening point (10 N)	153°C	150°C	120°C	—	145°C	ASTM D 1525 (ISO 306/A)

R scale utilizes 0.5 inch penetrator with 10 to 60 kgf (kilogram force) load which is suitable for plastics.
[a] Charpy notched impact strength measured by ISO 179 method.
[b] Shore hardness (Shore D).

particles formed in the first reactor, which exhibit a multiple structure, represented by the double-grain model proposed by Bukatov et al.,[26] and (2) the localization and distribution of EPR inside the preformed iPP matrix in the second reactor, which affect the impact properties of hiPP.[27]

Although there are many studies of laboratory-made hiPP, structural and morphological studies of commercial hiPP are very rare. Thus, studies of commercial hiPP are very important with respect to structure–property relationships.

In this study, the composition and chain structure of four commercial-grade hiPP, produced with spherical Ziegler–Natta catalyst, were studied by means of a TGEF method followed by Fourier transform infrared (FTIR) and differential scanning calorimetry (DSC) analysis of all of the fractions. Furthermore, the morphologies of these commercial hiPPs were evaluated with scanning electron microscopy (SEM) observations of the original and etched samples.

EXPERIMENTAL

Materials

The commercial polyolefin samples used in this study were heterophasic PP copolymer grades EPC40R and EPD60R (Arak Petrochemical Co., Arak, Iran), PP impact-copolymer-grade Moplene PPU 1752HL23 (Basell), PP impact-copolymer-grade PP 108MF10 (of SABIC), and iPP grade PI0800 (Bandar Imam Petrochemical Co., Iran). This PP homopolymer (PI0800) was used for infrared comparison. The samples were identified as EPC40R, EPD60R, HL23, 108MF10, and PI0800 in this study. The resins were analyzed as received without additive separation.

Temperature-gradient extraction fractionation

Because granulated polymers are not suitable for fractionation, the samples were dissolved in hot xylene (at 120°C) and were then precipitated by the addition of cold methanol, filtered, and dried *in vacuo*. These steps will erase any thermal history and create a standard thermal history for the samples. All of the hiPP samples were fractionated according to a TGEF procedure with a modified

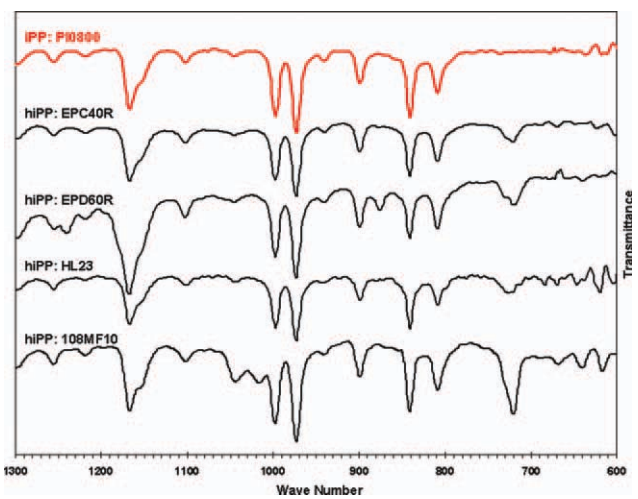

Figure 1 Comparison of the ATR–FTIR spectra of the iPP and hiPP samples in the 600–1300-cm^{-1} region. [Color figure can be viewed in the online issue, which is available at wileyonlinelibrary.com.]

TABLE II
TGEF Results for the hiPP Samples

	EPC40R				EPD60R				HL23				108MF10			
	Fraction mass (g)	C_2 (mol %)	C_2 (wt %)	C_2 (g) in fraction	Fraction mass (g)	C_2 (mol %)	C_2 (wt %)	C_2 (g) in fraction	Fraction mass (g)	C_2 (mol %)	C_2 (wt %)	C_2 (g) in fraction	Fraction mass (g)	C_2 (mol %)	C_2 (wt %)	C_2 (g) in fraction
Fr 1	0.1460	69.33	60.11	0.0878	0.1702	58.5	48.45	0.0825	0.2514	62.8	52.95	0.1331	0.4166	66.6	57.07	0.2378
Fr 2	0.0500	71.7	62.81	0.0314	0.0857	76.1	67.98	0.0583	0.0268	75.6	67.38	0.0181	0.1023	87.4	82.22	0.0841
Fr 3	0.0576	81	73.97	0.0426	0.0506	70.1	60.98	0.0309	0.0453	85.9	80.24	0.0363	0.1057	81.4	74.47	0.0787
Fr 4	0.0293	60.6	50.63	0.0148	0.0593	63.7	53.91	0.0320	0.0391	79.7	72.36	0.0283	0.0721	80.3	73.10	0.0527
Fr 5	0.0632	38.7	29.62	0.0187	0.0887	60	50.00	0.0444	0.0942	58.4	48.34	0.0455	0.1568	55	44.90	0.0704
Fr 6	0.6591	16.29	11.48	0.0757	0.1373	51	40.96	0.0562	0.4526	0	0	0	0.2109	0	0	0
Fr 7	1.0800	0	0	0	1.5102	0	0	0	1.1047	0	0	0	1.0423	0	0	0
Total	2.0852	—	—	0.2710	2.102	—	—	0.3043	2.0141	—	—	0.2613	2.1067	—	—	0.5237

Fractions 1–7 were extracted at 70, 80, 90, 100, 110, 120, and >120°C, respectively.

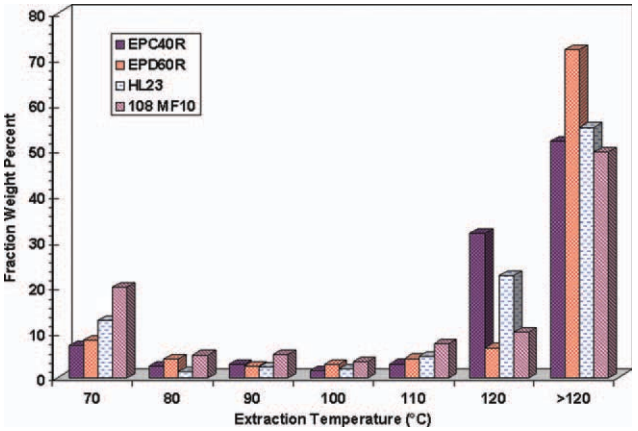

Figure 2 Fraction weight distributions of the hiPP samples. [Color figure can be viewed in the online issue, which is available at wileyonlinelibrary.com.]

Kumagawa extractor.[28] The fractionation solvent was *n*-octane, and seven fractions were collected from 2 g of each sample. The extraction temperatures were 70, 80, 90, 100, 110, 120, and greater than 120°C. The fraction at greater than 120°C was the residue in the extractor after fractionation at 120°C. Almost 0.1% antioxidant Irganox 1010 was added to the solvent before each separation step. After the concentration and precipitation of fractions (by the addition of cold acetone), pure fractions were obtained by washing and drying at 70°C *in vacuo*.

FTIR spectral characterization

FTIR spectra were acquired with a Bruker Equinox55 FTIR spectrophotometer (Ettlingen, Germany) equipped with a Deuterated Triglycine Sulfate (DTGS) detector and a Golden Gate micro-attenuated total reflectance (micro-ATR). Samples were introduced for micro-ATR–FTIR measurements without preparation. The band positions were obtained with Opus software

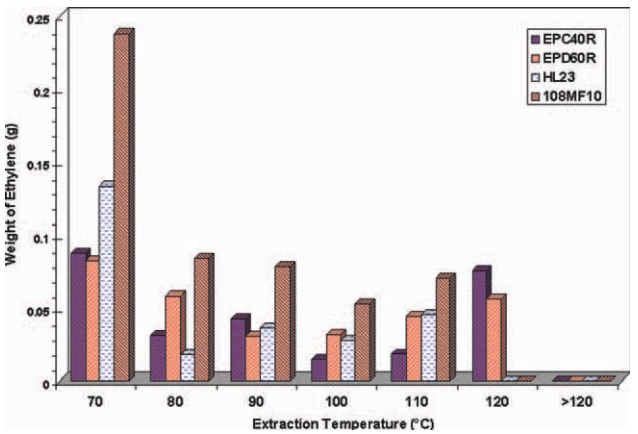

Figure 3 Ethylene content of fractions in the hiPP samples. [Color figure can be viewed in the online issue, which is available at wileyonlinelibrary.com.]

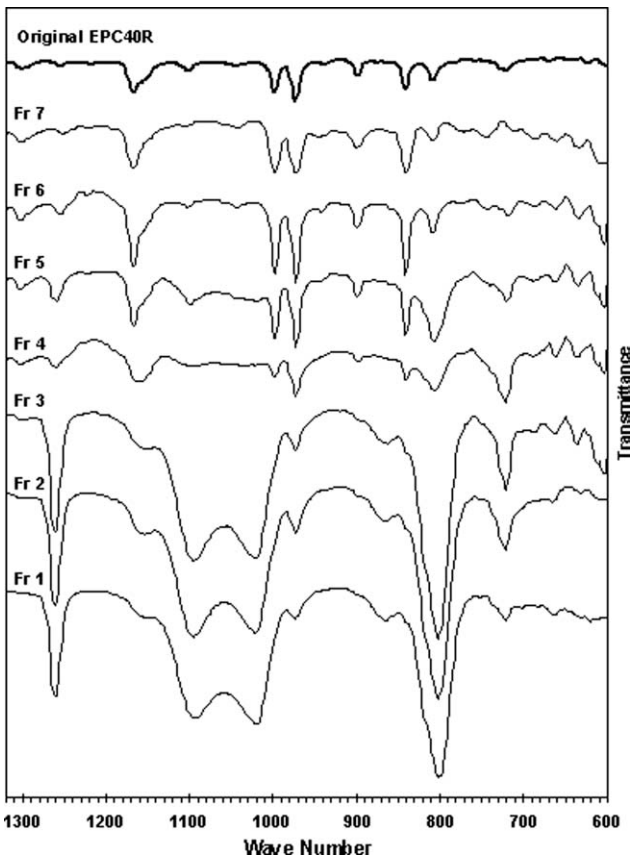

Figure 4 ATR–FTIR spectra of the EPC40R and its fractions in the 600–1320-cm^{-1} region.

(Ettlingen, Germany). The ethylene content in the copolymer fractions could be calculated according to the following equation on the basis of the FTIR spectra:[24]

$$\ln \frac{A_{1150}}{A_{720}} = 2.98 - 0.060C_2$$

where C_2 is the molar percentage of ethylene in the copolymer.

Thermal analysis

DSC analysis of the fractions and original samples were carried out with a TA DSC Q100 V9.0 (New Castle, DE) equipped with thermal analysis data acquisition software. The polymer samples (ca. 2 mg) were sealed in standard aluminum pans. First, we melted the sample by raising the temperature to 180°C, with the temperature kept at that level for 5 min to ensure complete melting and to remove the thermal history. The sample was then cooled to room temperature at a cooling rate of −10°C/min. After this, we recorded the melting endotherm by heating the sample directly to 230°C at a heating rate of +10°C/min.

Morphological analysis

The morphology and dispersion of the EPR phase in the iPP matrix of the hiPP samples were investigated with SEM with a Zeiss DSM 960A instrument (Oberkochen, Germany). The microtome-cut cross sections of the hiPP granules and etched samples (with xylene at 65°C) were coated with gold before the SEM observations.

Mechanical properties

Some important mechanical and physical properties of the resins were measured according to ASTM (or ISO) procedures (Table I).

RESULTS AND DISCUSSION

Overall structure and mechanical properties of the hiPP samples

In Table I, some of the mechanical and physical properties of iPP and hiPP samples used in this study, are listed. For the hiPP samples, the impact strengths were greater than that of iPP because they contained a disperse elastomeric phase inside the PP matrix; this improved the impact strength of the resin.

The attenuated total reflectance (ATR)–FTIR spectra of the iPP (homopolymer) and hiPP samples in the 600–1300-cm^{-1} region are shown in Figure 1.

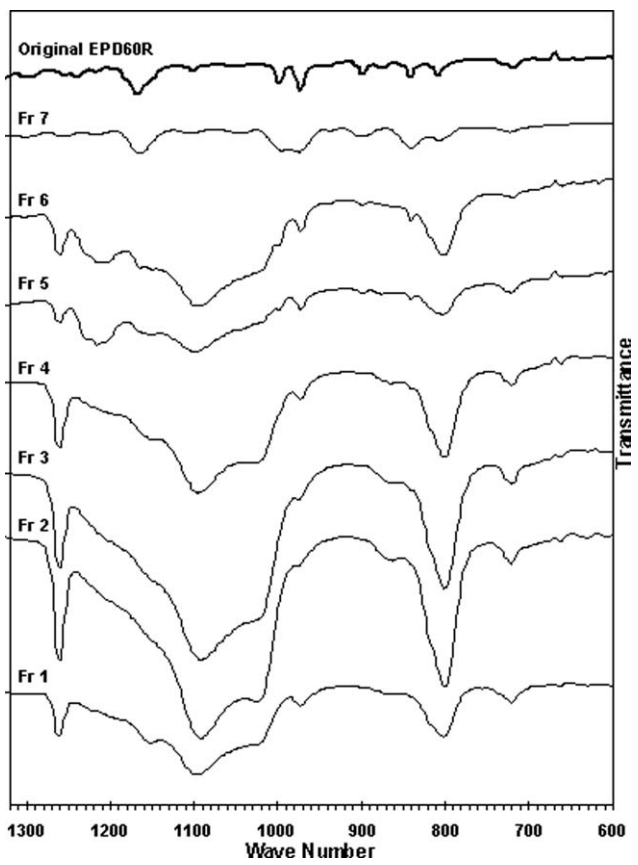

Figure 5 ATR–FTIR spectra of the EPD60R and its fractions in the 600–1320-cm^{-1} region.

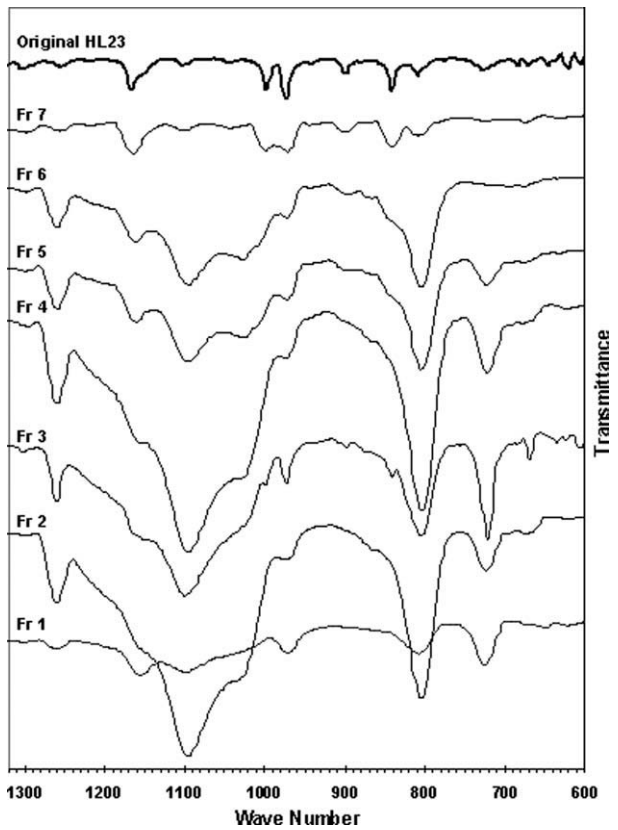

Figure 6 ATR–FTIR spectra of the HL23 and its fractions in the 600–13,200-cm^{-1} region.

The spectra are very similar except for the 720-cm^{-1} band in the hiPP samples spectra due to ethylene sequence;[29] this means that there were ethylene segments or blocks in their structure. The absorbance of the 720-cm^{-1} band in the 108MF10 grade was greater than the others (with respect to the 1150-cm^{-1} band) because, as will be shown later, it contained the maximum ethylene content among the other hiPP samples.

Fractionation

A sample of hiPP (2 g) for each grade was fractionated by TGEF into seven fractions. The results of the fractionation of samples and the ethylene content for each fraction are given in Table II. (The overweight was due to the antioxidant added.) The weight distributions of the fractions and their ethylene content in the hiPP samples are shown in Figures 2 and 3, respectively. It is obvious that for all of the hiPP samples, the fractions extracted at 120 and >120°C constituted the main portion of the blend, whereas the other fractions extracted at lower temperatures (70–110°C) accounted for only about 17–40 wt % of the resin. However, these fractions played a very important role in the impact strength of the resin, as discussed later. Figure 3 shows that the main portion of ethylene in the hiPP samples was located in fraction 1, which was extracted at the lowest fractionation temperature. Because fractionation with the TGEF technique was performed according to the crystallinity of the fractions,[28] the fractions extracted at lower temperatures were amorphous copolymers, and the fractions extracted at higher temperatures were semicrystalline to highly crystalline iPP.

Chain structure of the fractions

All of the TGEF fractions obtained from the hiPP samples were analyzed with ATR–FTIR spectroscopy and DSC to investigate their microstructures. The ATR–FTIR spectra of the seven fractions and the original resin for all of the hiPP samples are shown in Figures 4–7.

The spectra of fractions 1–3 for EPC40R and 1–6 for other grades were very similar to the ATR–FTIR spectra of statistical ethylene–propylene copolymers,[21] and the spectra of fraction 7 in all of the samples were very similar to those of iPP (Fig. 1). As shown in Table II, the absorbance of the ethylene sequence band at 720 cm^{-1} in fractions 1–5 was very high with respect to the 1150-cm^{-1} band. This absorbance was very low or vanished in the spectra

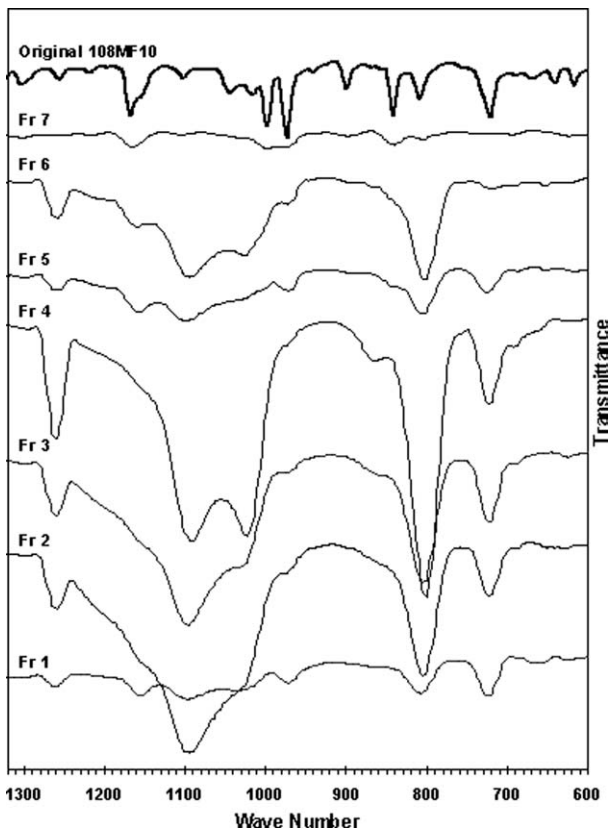

Figure 7 ATR–FTIR spectra of the 108MF10 and its fractions in the 600–1320-cm^{-1} region.

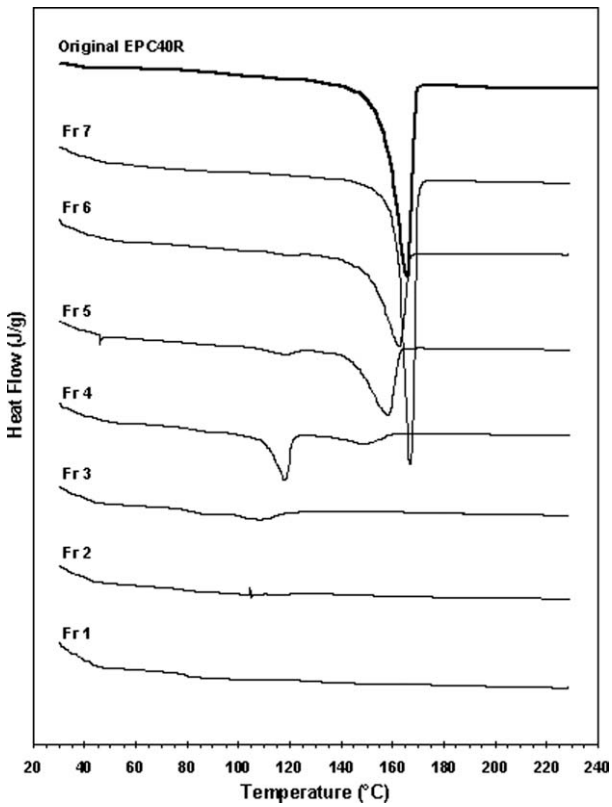

Figure 8 DSC thermograms of the EPC40R and its fractions.

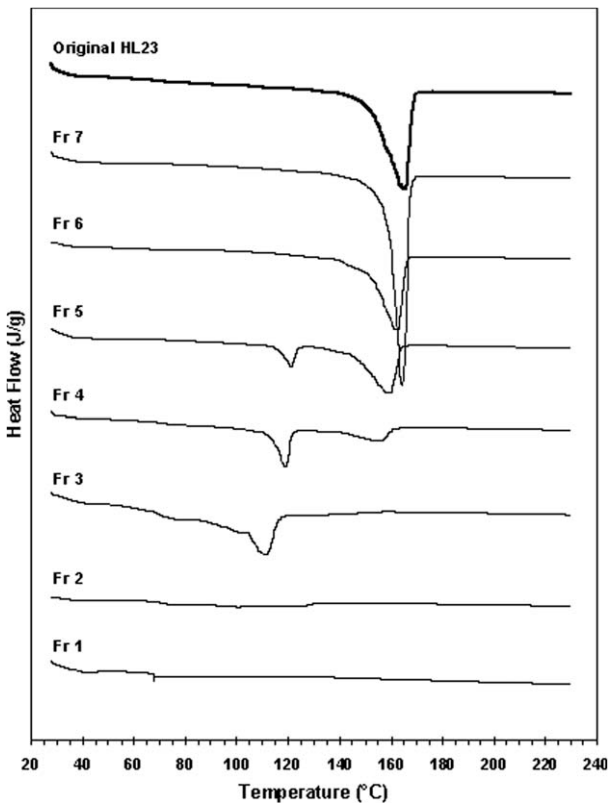

Figure 10 DSC thermograms of the HL23 and its fractions.

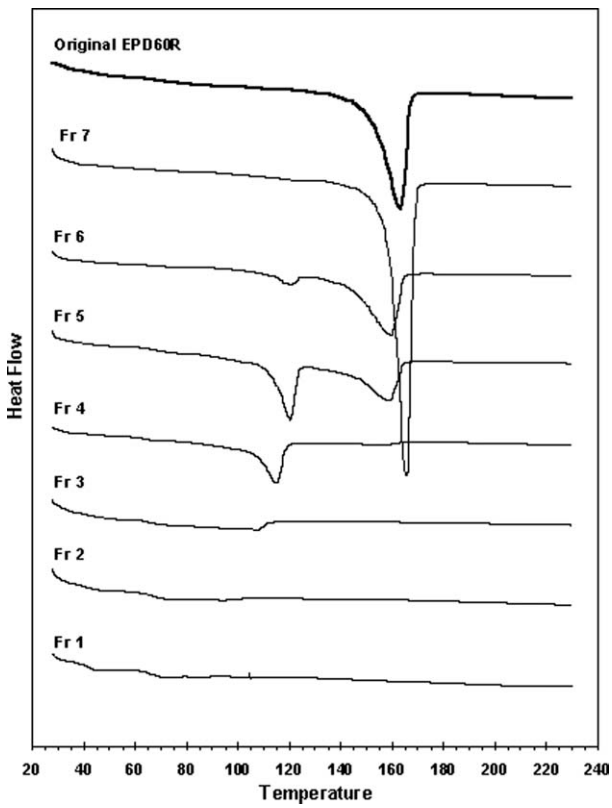

Figure 9 DSC thermograms of the EPCD60R and its fractions.

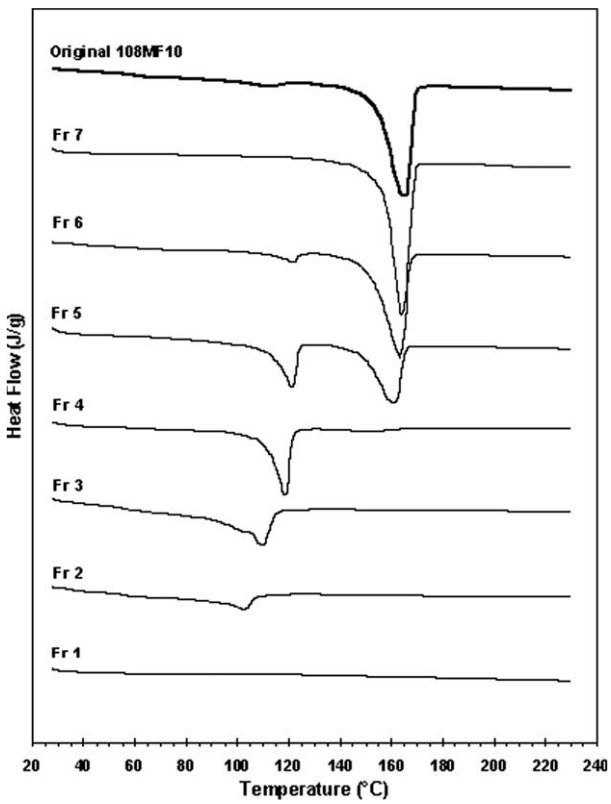

Figure 11 DSC thermograms of the 108MF10 and its fractions.

TABLE III
DSC Data for EPC40R and Its Fractions

Sample	Extraction temperature (°C)	Fraction concentration (wt %)	T_g (°C)[a]	T_m (°C)[b]	ΔH_f (J/g) (T_m)[c]	Comment
Fr 1	70	7.00	79.7	—	—	—
Fr 2	80	2.40	79.8	— (104.7, 116.6)	— (~ 0)	Negligible
Fr 3	90	2.76	81.3	— (108.3)	— (7.6)	Very weak
Fr 4	100	1.41	—	148.9 (118.2)	11.4 (37.3)	Two endotherms
Fr 5	110	3.03	—	158.3 (118.1)	64.6 (4.9)	Two endotherms
Fr 6	120	31.61	—	162.7	91.0	Sharp
Fr 7	>120	51.79	—	166.7	145.2	Very sharp
EPC40R	—	—	—	165.9	69.3	Sharp

T_m, melting temperature.
[a] Glass-transition temperature for the elastomeric fractions.
[b] Numbers in parentheses are the temperatures of the polyethylene endothermic peaks.
[c] Enthalpy of fusion at T_m. The numbers in parentheses are the melting enthalpies of the polyethylene peaks.

of fractions 6 and 7, which were considered to be the PP homopolymer.

Fractions 1–5 did not show the pure crystalline band at 730 cm^{-1} because this band was sharp and separate from the 720-cm^{-1} band, whereas the 733-cm^{-1} band appeared as a shoulder on the 720-cm^{-1} band. The absorptions at 841 and 998 cm^{-1} due to methyl rocking modes associated with the threefold helical structure of iPP were not seen in the ATR–FTIR spectra of fractions 1–3 (for the EPC40R) and 1–5 (for the other three grades); this was further evidence that these fractions were completely amorphous. The first sign of these helix bands appeared in fractions 4 (for the EPC40R) and 6 (for the other samples). In the spectra of fraction 6, extracted at 120°C, the ethylene sequence band was very weak, and in that of fraction 7, extracted at >120°C, it did not appear, but the helix bands of iPP in the spectra of both of these two fractions were present. In other words, they were actually iPP.

The strong absorption at 800 cm^{-1} for the initial fractions was assigned to the chains in nonhelical conformation (amorphous structure).[30] This band transformed to a rather week band at 806 cm^{-1} in the spectra of fractions 6 and 7, which was assigned to methylene rocking [$\gamma_r(CH_2)$], backbone carbon–carbon stretching [ν(C—C chain)], and carbon–methyl stretching [ν(C—CH_3)] vibrations, and represented the helical structure in crystalline regions. There was also a rather complete explanation of the ATR–FTIR spectra of these fractions in our previous work.[31]

The DSC thermograms of all of the fractions in the range 30–230°C are shown in Figures 8–11, and the DSC data are also summarized in Tables III–VI. As shown in Figures 8–11, the thermograms were very similar for four samples. This could be considered proof for TGEF repeatability for the fractionation of similar samples. For all of the samples, fractions 1 and 2 did not show any melting endothermic peaks, and in fraction 3, there was a very weak peak at about 110°C; this was probably due to very small and thin lamellae of polyethylene crystallites. The first sign of existence of crystalline polyethylene and PP together was observed in fraction 4 (except for the EPD60R sample). This fraction, extracted at 100°C, also had a very large polyethylene melting endotherm; this indicated that it contained long segments of ethylene in the backbone, which were

TABLE IV
DSC Data for EPD60R and Its Fractions

Sample	Extraction temperature (°C)	Fraction concentration (wt %)	T_g (°C)[a]	T_m (°C)[b]	ΔH_f (J/g) (T_m)[c]	Comment
Fr 1	70	8.1	65.1	—	—	—
Fr 2	80	4.08	66.7	— (96.3)	— (2.0)	Negligible
Fr 3	90	2.41	65.2	— (108.2)	— (11.3)	Very weak
Fr 4	100	2.82	65.5	— (115.2)	— (28.5)	Weak
Fr 5	110	4.22	—	159.1 (120.1)	30.1 (29.4)	Two endotherms
Fr 6	120	6.53	—	159.8 (119.8)	53.1 (5.7)	Two endotherms
Fr 7	>120	71.85	—	165.3	140.0	Very sharp
EPD60R	—	—	—	163.2	73.4	Sharp

T_m, melting temperature.
[a] Glass-transition temperature for elastomeric fractions.
[b] Numbers in parentheses are the temperature of the polyethylene endothermic peaks.
[c] Enthalpy of fusion at T_m. The numbers in parentheses are the melting enthalpy of polyethylene peaks.

TABLE V
DSC Data for HL23 and Its Fractions

Sample	Extraction temperature (°C)	Fraction concentration (wt %)	T_g (°C)[a]	T_m (°C)[b]	ΔH_f (J/g) (T_m)[c]	Comment
Fr 1	70	12.48	66.5	—	—	—
Fr 2	80	1.33	70.3	— (100.0, 124.6)	— (3.1, 2.9)	Negligible
Fr 3	90	2.25	67.3	—, (111.4)	— (26.4)	Has shoulder
Fr 4	100	1.94	71.8	155.5, (118.8)	20.1, (24.9)	Two endotherms
Fr 5	110	4.68	—	159.5, (120.9)	49.6, (13.0)	Two endotherms
Fr 6	120	22.47	—	162.4	96.4	Sharp
Fr 7	>120	54.85	—	164.1	112.3	Very sharp
HL23	—	—	—	165.2	68.0	Sharp

T_m, melting temperature.
[a] Glass-transition temperature for the elastomeric fractions.
[b] Numbers in parentheses are the temperature of the polyethylene endothermic peaks.
[c] Enthalpy of fusion at T_m. Numbers in parentheses are the melting enthalpy of the polyethylene peaks.

enough to form different lamellae with medium thicknesses. From the DSC data and the ATR–FTIR results, we concluded that this fraction was an ethylene–propylene segmented copolymer (multiple-block copolymer), which was only about 1.41–3.42 wt % of the resins (Table II). All of the hiPP samples showed the polyethylene and PP endotherms in fraction 5, but the PP endotherms were much larger than that of fraction 4. This is obvious in Table II, where it is shown that for all samples, fraction 4 had a greater ethylene content than fraction 5. Again, by a combination of the DSC and ATR–FTIR spectra for fraction 5, we concluded that it was an ethylene–propylene block copolymer with a higher propylene content. (Note that fractions 5 was extracted at 10°C higher than fraction 4.) The amounts of fraction 5 in the resins were about 3.03–7.44 wt %. In the DSC traces of fractions 4, 5, and 6, the polyethylene endotherms gradually decreased, and in that of fraction 7, it did not appear. In other words, for the fractions extracted above 90°C, as the temperature increased, the polyethylene crystalline content decreased, and the PP crystalline content increased. The PP in fractions 6 and 7 was highly crystalline and, because these two final fractions constituted 60–80 wt % of the hiPP samples, they could be considered as the iPP matrix. Fraction 7 in all samples showed a very sharp and strong melting endotherm, much stronger than that of the original resins.

Although the existence of EPR in hiPP was the main factor that affected the impact resistance or toughness of the resin, its compatibility and interface with the iPP matrix had significant consequences in the impact–rigidity (or toughness–stiffness) balance of the resin.[11,32]

It is known that in hiPP, the ethylene–propylene segmented copolymer (fraction 4) and the ethylene–propylene block copolymer (fraction 5) act as compatibilizers between EPR and the iPP phases; this improves the adhesion between them.[12,25,33] Therefore, the role of these semicrystalline ethylene–propylene copolymers is very important in hiPP. The very low content of these components in the commercial hiPPs under investigation (except

TABLE VI
DSC Data for 108MF10 and Its Fractions

Sample	Extraction temperature (°C)	Fraction concentration (wt %)	T_g (°C)[a]	T_m (°C)[b]	ΔH_f (J/g) (T_m)[c]	Comment
Fr 1	70	19.78	56.9	—	—	—
Fr 2	80	4.86	58.6	— (103)	— (15.8)	Weak
Fr 3	90	5.02	58.6	— (110.1)	— (32.3)	Has shoulder
Fr 4	100	3.42	—	155.6 (118.5)	3.9 (68.2)	Negligible endotherm for PP
Fr 5	110	7.44	—	160.7, (121.1)	41.1, (27.4)	Two endotherms
Fr 6	120	10.01	—	162.8, (121.9)	75.6, (6.2)	Two endotherms
Fr 7	>120	49.48	—	163.8	116.2	Very sharp
108MF10	—	—	—	165.3	60.3	Sharp

T_m, melting temperature.
[a] Glass-transition temperature for elastomeric fractions.
[b] Numbers in parentheses are the temperature of polyethylene endothermic peaks.
[c] Enthalpy of fusion at T_m. Numbers in parentheses are the melting enthalpy of the polyethylene peaks.

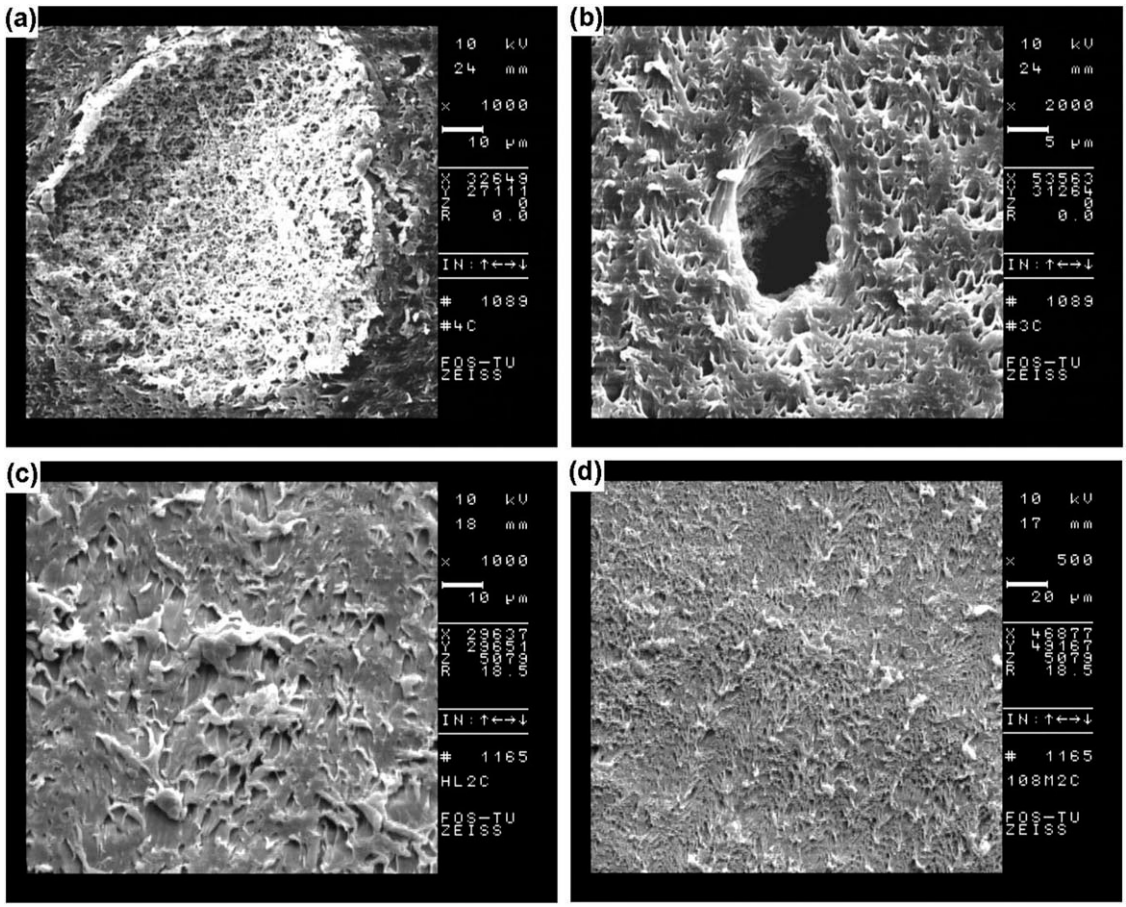

Figure 12 SEM micrographs of EPR removed cross section of etched samples: (a) EPC40R, (b) EPD60R, (c) HL23, and (d) 108MF10.

108MF10) indicated that the EPR particles did not adhere well to the matrix, so they could not work properly as an impact modifier.

Morphological study

For an elastomeric impact modifier to work properly, it is essential to have a suitable size and distribution inside the matrix. In fact, a smaller amount of an impact modifier with submicrometer size that is completely distributed through the matrix can act as a great amount of it with a large size and bad distribution. Therefore, it is possible that earns a specific impact resistance with a smaller amount of elastomeric phase, which indicates a lesser loss of matrix stiffness.

By comparison of the SEM micrographs of the original samples and etched samples, the distribution and morphology of the dispersed phase and the matrix can be easily understood. Various solvents can be used to remove the EPR phase, such as boiling *n*-heptane,[24] boiling *n*-hexane,[15] toluene (room temperature under ultrasound),[12] and xylene (room temperature).[34] In this study, xylene at 65°C (24 h) was used to remove the EPR phase from the microtome-cut samples. Figure 12 shows SEM micrographs of the cross section of samples etched at 65°C. These micrographs demonstrated the porous nature of the iPP matrix after the removal of the EPR phase. In the case of EPC40R and EPD60R, we observed that the distribution of the EPR particles in the matrix was not good (especially for EPC40R), whereas the other two grades had a fair distribution of elastomer inside the matrix. The size of EPR particles was also an important factor. As these particles were smaller, the interfaces between them and the matrix were larger, and their effect on improving the impact resistance of the resin was greater. As shown in Figure 12(a,b), the sizes of the elastic domains in the EPC40R and EPD60R were about 60 and 10 μm, respectively, whereas the favored size for good toughening of a material should be in the range 0.1–0.6 μm.[12] However, it seemed that the EPR phase in the other two grades was completely dispersed and did not coagulate to form distinct particles.

CONCLUSIONS

The composition, chain structure, and morphology of four commercial hiPPs were investigated with TGEF, ATR–FTIR spectroscopy, DSC, and SEM. The

following comments could be made with regard to the fractionation of hiPP by TGEF:

1. There were four structurally different components in the hiPP samples: an EPR elastomeric phase, an ethylene–propylene segmented (multiblock) copolymer, an ethylene–propylene block copolymer, and the iPP matrix.
2. The contents of the ethylene–propylene segmented copolymer and the ethylene–propylene block copolymer in the commercial hiPP resin studied were very low.
3. Because the ethylene–propylene segmented copolymer adhered to the EPR to the matrix and the ethylene–propylene block copolymer compatibilized it with the matrix, the low content of these fractions in the commercial hiPP strongly reduced the effect of the elastomeric phase. In fact, the 108MF10 grade, which had the largest amount of these copolymers, also had the best impact strength at low temperature (see Table I).
4. To obtain the best impact–rigidity balance, the content of semicrystalline ethylene–propylene copolymers in commercial products must be increased. It has been suggested that the amount of these copolymers in hiPP must be comparable with the EPR itself.[12,25]

Furthermore, morphological studies with SEM showed that the distribution of EPR particles in the matrix for EPC40R was not good, and it was obvious that these particles aggregated in this sample. On the other hand, the EPR particles in the EPC40R and EPD60R were very large (because of aggregation). This means that the interface between them and the matrix was very small; this further minimized the role of the elastomeric phase (and its content). Because it was very critical for hiPP to reach the impact–rigidity balance with a minimum content of EPR, the size of EPR particles in commercial hiPP had to be decreased, and they needed to be distributed more homogeneously in the resin.

The authors are grateful to the Tehran University Research Council. They also thank the Laboratory of Electron Microscopy of the College of Science, University of Tehran.

References

1. Moore, E. O., Jr. Polypropylene Handbook; Hanser: Munich, 1996.
2. Wu, S. Polym Eng Sci 1990, 30, 753.
3. Van der Wal, A.; Mulder, J. J.; Oderkerk, J.; Gaymans, R. J. Polymer 1998, 39, 6781.
4. Liang, J. Z.; Li, R. K. Y. J Appl Polym Sci 2000, 77, 409.
5. Galli, P.; Vecellio, G. Prog Polym Sci 2001, 26, 1287.
6. Cecchin, G.; Morini, G.; Pelliconi, A. Macromol Symp 2001, 173, 195.
7. Jang, B. Z.; Uhlman, D. R.; Vander Sande, J. B. Polym Eng Sci 1985, 25, 643.
8. Binsbergen, F. L.; Delarge, B. G. M. Polymer 1970, 11, 309.
9. Lin, Y.; Chen, H.; Chan, C. M.; Wu, J. Macromolecules 2008, 41, 9204.
10. Hoygshi, K.; Morioka, T.; Toki, S. J Appl Polym Sci 1993, 48, 411.
11. Fu, Z. S.; Xu, J. T.; Zhang, Y. Z.; Fan, Z. Q. J Appl Polym Sci 2005, 97, 640.
12. Fu, Z. S.; Fan, Z. Q.; Zhang, Y. Q.; Feng, L. X. Eur Polym J 2003, 39, 795.
13. Simonazzi, T.; Cecchin, G.; Mazzullo, S. Prog Polym Sci 1991, 16, 303.
14. Galli, P.; Haylock, J. C. Makromol Chem Macromol Symp 1992, 63, 19.
15. Urdampilleta, I.; Gonzalez, A.; Iruin, J. J., de la Cal, J. C.; Asua, J. M. Macromolecules 2005, 38, 2795.
16. Mirabella, F. M., Jr. Polymer 1993, 34, 1729.
17. de Goede, E.; Mallon, P.; Pasch, H. Macromol Mater Eng 2010, 295, 366.
18. Sacchi, M. C.; Fan, Z. Q.; Forlini, F.; Tritto, I.; Locatelli, P. Macromol Chem Phys 1994, 195, 2805.
19. Fu, Z. S.; Fan, Z. Q.; Zhang, Y. Z.; Xu, J. T. Polym Int 2004, 53, 1169.
20. Paxson, J. R.; Randall, J. C. Anal Chem 1979, 50, 1777.
21. Wei, P. E. Anal Chem 1961, 33, 215.
22. Tritto, I.; Fan, Z. Q.; Locatelli, P.; Sacchi, M. C.; Camurati, I.; Galimberti, M. Macromolecules 1995, 28, 3342.
23. Hongjun, C.; Xiaolie, L.; Xiangxu, C.; Dezhu, M.; Jianmin, W.; Hongsheng, T. J Appl Polym Sci 1999, 71, 93.
24. Fan, Z. Q.; Zhang, Y. Q.; Xu, J. T.; Wang, H. T.; Feng, L. X. Polymer 2001, 42, 5559.
25. Hongjun, C.; Xiaolie, L.; Xiangxu, C.; Dezhu, M.; Jianmin, W.; Hongsheng, T. J Appl Polym Sci 1999, 71, 103.
26. Bukatov, G. D.; Zaikovskii, V. I.; Zakharov, V. A.; Kryukova, G. N.; Fenelonov, V. B.; Zagrafskaya, R. V. Polym Sci USSR 1982, 24, 599.
27. Dong, Q.; Wang, X. F.; Fu, Z. S.; Xu, J. T.; Fan, Z. Q. Polymer 2007, 48, 5905.
28. Sacchi, M. C.; Fan, Z. Q.; Forlini, F.; Tritto, I.; Locatelli, P. Macromol Chem Phys 1994, 195, 2805.
29. Andreassen, E. In Polypropylene: An A–Z Reference; Karger-Kocsis, J., Ed.; Kluwer Academic: Dordrecht, The Netherlands, 1999; p 320.
30. Khafagy, R. M.; Badr, Y. A. J Polym Sci Part B: Polym Phys 2005, 43, 2829.
31. Mahdavi, H.; Enayati Nook, M. Polym Int 2010, 59, 1701.
32. Chen, J. H.; Zhong, J. C.; Cai, Y. H.; Su, W. B.; Yang, Y. B. Polymer 2007, 48, 2946.
33. Jiang, T.; Chen, Y.; Ning, Y.; Kuang, D.; Qu, G. J Appl Polym Sci 2006, 101, 1386.
34. Chen, Y.; Chen, Y.; Chen, W.; Yang, D. Polymer 2006, 47, 6808.